Rare Met. (2013) 32(5):448–452
DOI 10.1007/s12598-013-0157-3

RARE METALS
www.editorialmanager.com/rmet

Phase transformation behaviors and mechanical properties of $Ti_{50}Ni_{49}Fe_1$ alloy with severe plastic deformation

Wen Ma*, Bin Chen, Fu-Shun Liu, Qing Xu

Received: 6 August 2013 / Revised: 21 August 2013 / Accepted: 23 September 2013 / Published online: 30 October 2013

Abstract In this work, transformation behaviors and mechanical properties of cold-rolled shape memory alloy $Ti_{50}Ni_{49}Fe_1$ by severe plastic deformation (SPD) were intensively investigated. The phase transformation behaviors, phase analysis, and microstructures were characterized by differential scanning calorimetry (DSC), X-ray diffraction (XRD), and transmission electron microscopy (TEM), respectively. Tensile testing was performed to analyze the effect of SPD on the mechanical properties and shape memory of $Ti_{50}Ni_{49}Fe_1$ alloy. When the thickness reduction is beyond 30 %, the martensitic transformation is suppressed. After cold-rolling, the alloy is mainly composed of B2 parent phases with some stress-induced martensitic B19′ phases, and high density of dislocations are generated and the grains are obviously refined. The yield stress σ_b significantly raises from 618 MPa of 0 % cold rolling to 1,338 MPa of 50 % SPD. Shape-memory effect increases from 6.5 % without cold rolling to 8.5 % after 30 % SPD, ascribed to the induced defects in cold rolling. Those results indicate that $Ti_{50}Ni_{49}Fe_1$ alloy has improved mechanical properties and potential commercial applications after SPD.

W. Ma*
Division of Science and Technology Information, General Research Institute for Nonferrous Metals, Beijing 100088, China
e-mail: mawen19860507@126.com

W. Ma, B. Chen, F.-S. Liu
School of Material Science and Engineering, Beijing University of Aeronautics and Astronautics, Beijing 100191, China

Q. Xu
Metrology and Phsico-Chemical Institute, Capital Aerospace Machinery Company, Beijing 100076, China

Keywords TiNiFe alloy; Cold-rolling; Severe plastic deformation (SPD); Shape memory effect

1 Introduction

Owing to its outstanding shape memory effect, pseudoelasticity and excellent mechanical properties, TiNi-based shape memory alloy is renowned as quite appealing materials and are now being practically used as functional materials for pipe couplings, antennae for satellites, various actuators, medical implants, and guide wires [1, 2]. The strength of shape memory alloys is a extremely vital parameter in the practical application. If the applying stress exceeds the strength of the raw materials that can bear, it may lead to the fail of the parts [3].

It is well known that the means of strengthening the binary Ti–Ni alloy can be classified as followings: aging after solution treatment (Ni >50.5 at% practically) [4, 5] and specific thermo-mechanical treatments, i.e., annealing following cold working (Ni <50.5 at% practically) [6], thermal and/or stress cycling [7, 8]. SPD is a novel technology used to strengthen raw materials. There are some reports of this method. Valiev et al. [9–11] found that it can obviously improve both tensile strength and elongation of by fining grains employing SPD. Brailovski et al. [12–14] investigated the influence of thermo-mechanical method on Ti–50.0 at% Ni alloys. They obtained alloy with average grain size of 60–80 nm and advanced recovery strain of 8 % and recovery stress of 1,400 MPa applying SPD and post-deformation annealing. However, there are few reports about the influence of SPD on the TiNiFe ternary alloy. This paper investigated the influence of SPD on the TiNiFe alloy, improved both yield stress and shape-memory effects of TiNiFe shape

memory alloys, while the TiNiFe alloy is remained relative high elongation.

2 Experimental

Four ingots of quaternary alloys with the nominal compositions of $Ti_{50}Ni_{49}Fe_1$ (at%) were prepared by induction melting a mixture of 99.7 % Ti, 99.7 % Ni, and 99.99 % Fe in a high frequency vacuum furnace. Ingots were remelted four times and then homogenized in evacuated quartz tubes at 850 °C for 24 h. Then ingots were hot-rolled into plates with different thicknesses, following with cold-rolling into plates with thickness of 1.1 mm, insuring thickness reduction to be 0 %, 15 %, 30 %, and 50 %, marked as CR0 %, CR15 %, CR30 %, and CR50 % in this work, respectively. Specimens for measurements were spark cut from the plates.

The phase transformation temperatures were determined by a Q2000 differential scanning calorimetry (DSC). The temperatures ranged from −90 to 100 °C, with a heating/cooling rate of 10 °C·min^{-1}. Phase identification was performed in a Rigaku D/max-rB X-ray diffractometer (XRD) with Cu Kα radiation ($\lambda = 0.15405$ nm, $2\theta = 20°$–90°) and a scan speed of 6 (°)·min^{-1}. The microstructures of $Ti_{50}Ni_{49}Fe_1$ alloy were performed by a transmission electron microscopy (TEM, FEI Quanta 200F). Mechanical properties were detected on a MTS model 880 with a strain rate of 5.6×10^{-4} at room temperature (25 °C). Shape-memory effect was performed on a tensile test machine (MTS model 880) at −196 °C and then pre-strained alloys were heated to 120 °C to measure the recovery strain.

3 Results and discussion

3.1 Effect of cold-rolling on phase transformation properties

Figure 1 shows the transformation behaviors of $Ti_{50}Ni_{49}Fe_1$ alloy with CR0 %, CR15 %, CR30 %, and CR50 %. It can be seen that $Ti_{50}Ni_{49}Fe_1$ alloy exhibits two exothermic peaks (presenting A → R and R → B19′ transformations, respectively) and one endothermic peak (presenting M → A transformation). It is evident that the peaks of both A → R and R → B19′ transformations are significantly broadened and weakened by SPD. As shown in Fig. 1, the alloy with CR15 % exhibits A → R, R → B19′, and M → A transformations. With more SPD (up to CR30 %), however, R → B19′ transformation is suppressed, as shown in Fig. 1.

Meanwhile, A → R transformation still exists, with widening transformation peaks. This can be ascribed to the large amount of defects (such as dislocation) producing during cold rolling. Defects hinder the movement of the interface between two phases in transformation. In such a case, the transformation peaks get wider and weaker, and vanish eventually. The lattice distorsion of R → B19′ is larger than that of A → R [15], as a result, the peak of R → B19′ transformation disappears while that of A → R still remains weak [16].

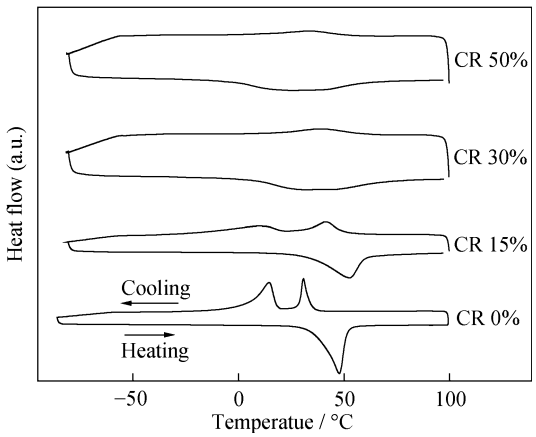

Fig. 1 DSC curves of $Ti_{50}Ni_{49}Fe_1$ alloy with different cold-rollings

3.2 XRD analysis

Figure 2 shows the XRD patterns of $Ti_{50}Ni_{49}Fe_1$ alloy after different cold-rollings at room temperature. It can be seen that at room temperature, $Ti_{50}Ni_{49}Fe_1$ alloy with CR0 % mainly consists of B2 phase and a small amount of R phase. But after cold rolling, a small amount of martensites (M) appear. The martensitic start transformation temperature (M_s) of $Ti_{50}Ni_{49}Fe_1$ is 18 °C, as shown in Fig. 1. Some weak peaks are observed at the 2θ of 29°, 31°, and 33°, and the intensities of them increase with the increase of SPD, as shown in Fig. 2. It is confirmed that these peaks corresponds to martensites' peak according the PDF card. Therefore, although the M_s is lower than room temperature (18 °C), the cold rolling results in stress induced martensite

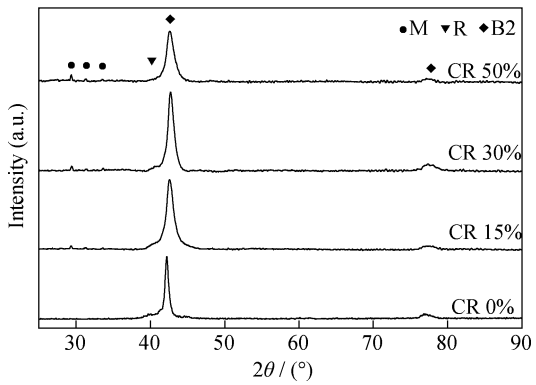

Fig. 2 XRD patterns of $Ti_{50}Ni_{49}Fe_1$ alloy after different cold-rollings

transformation and M phase remains in the alloys with cold rolling at room temperature.

Meanwhile, it can be seen from XRD patterns in Fig. 2 that $(110)_{B2}$ is observed in 42.2° without cold rolling, but shifted to right in 42.6° with cold rolling. The peak of $(110)_{B2}$ is obviously widened with the increase of cold rolling. The widened peak $(110)_{B2}$ might be caused by two reasons [15]: (1) lattice defects, resulting from the introduction of much residual stress, influences the XRD patterns; (2) the grains are refined because of SPD after which some grains are broken. According to Debye–Scherrer formula:

$$D = K\lambda/B\cos\theta, \quad (1)$$

where K is constant, 0.89; D is the particle size, nm; B is the integral half width, rad; θ is the diffraction degree, (°); and λ is the wave length of X-ray, nm. It can be calculated from Eq. (1) that after the grains are refined, smaller D will result in the obvious widened peak (larger θ) of XRD patterns.

3.3 Effect of cold-rolling on microstructures

Figure 3 shows the TEM images of $Ti_{50}Ni_{49}Fe_1$ alloy after CR0 % and CR50 %. Comparing with Fig. 3a, it is apparent from the Fig. 3b that a relatively high density of dislocation is introduced via cold rolling, as shown by the arrow in Fig. 3b. The corresponding selected area diffraction pattern (SADP) with a beam direction of $(111)_{B2}$ is shown in the insert. Diffraction rings are observed. The inner rings corresponds to (110) planes of the B2 phase, with the outer (211) and (220) of the B2 phase, respectively, in which the grains of the cold-rolled alloys are obviously refined.

3.4 Effect of cold-rolling on mechanical properties

Figure 4a shows the stress–strain curves of $Ti_{50}Ni_{49}Fe_1$ alloys with different cold-rolling reductions. For comparison's sake, the magnitudes of σ_b, σ_S and elongation were plotted against thickness reduction in Fig. 4b. As illustrated in Fig. 4, σ_b increases remarkably with cold-rolling rate increasing, from 618 to 1,338 MPa with CR0 % to CR50 %. Also, σ_S increases with cold rolling increasing. In contrast, the elongation of the alloys exhibits a gradual decrease with cold rolling increasing, as revealed in Fig. 4b. $Ti_{50}Ni_{49}Fe_1$ alloy with CR15 % exhibits a slight decrease (from 25 % of alloy with CR0 % to 24 %). Nevertheless, alloys applied more SPD display sharp declining. For example, $Ti_{50}Ni_{49}Fe_1$ alloy with SPD of 30 % and 50 % remain elongation of 16 % and 12 %, respectively.

This can be ascribed to two following reasons: (1) the high density of dislocation accompanied with severe cold deformation impedes the movement of the particular dislocation; (2) the refined grains result in a mass of grain boundaries which can effectively hinder the slip of dislocations.

For polycrystalline materials, the Hall–Petch equation can describe the relationship between yield strength and grain size [17]. Yield strength increases with a decreasing grain size according to the following equation:

$$\sigma = \sigma_0 + kd^{-1/2}, \quad (2)$$

where σ is the yield stress, and d is the average grain size. Typically, σ_0 is rationalized as either a frictional stress resisting the motion of gliding dislocations or as an internal back stress. k is the Hall–Petch slope, which is considered

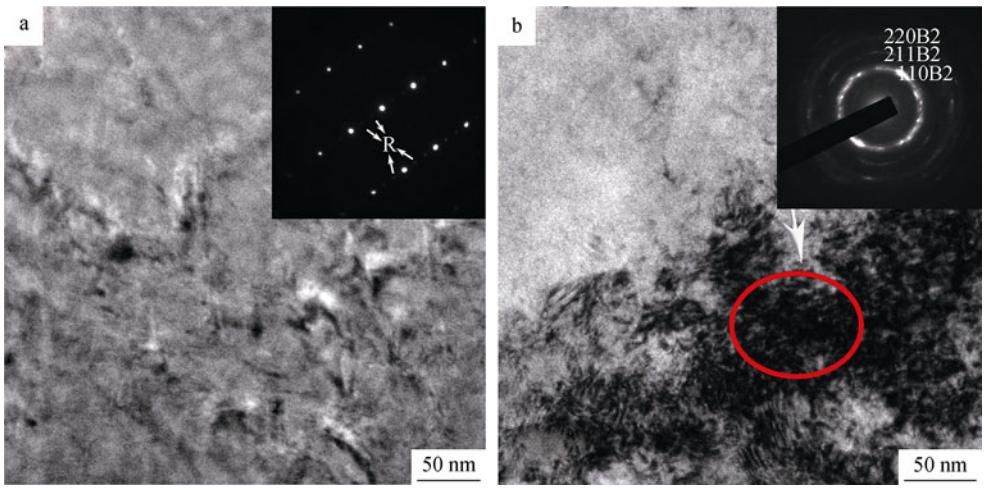

Fig. 3 TEM bright field images and $(111)_{B2}$ zone axis selected area electron diffraction (SAED) images of $Ti_{50}Ni_{49}Fe_1$ alloy after **a** CR 0 % and **b** CR 50 %

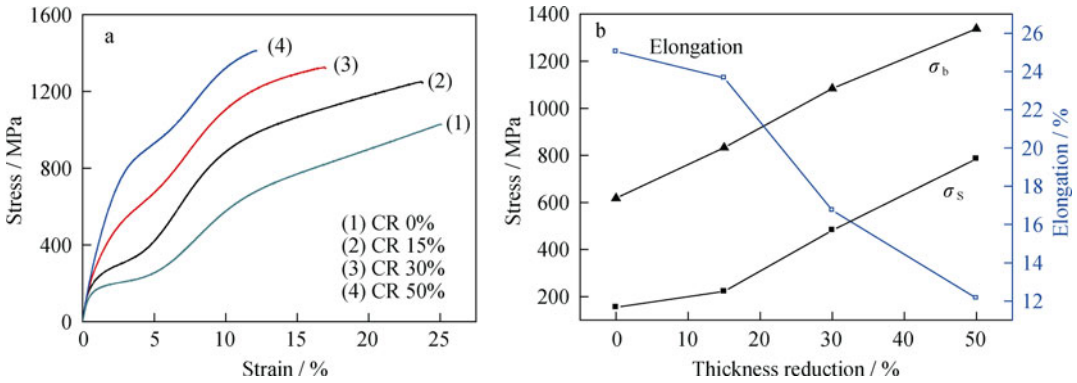

Fig. 4 Strain–stress curves of $Ti_{50}Ni_{49}Fe_1$ alloys with different cold-rolling reductions **a** and thickness reduction dependence of σ_S, σ_b and elongation in the $Ti_{50}Ni_{49}Fe_1$ alloys **b**

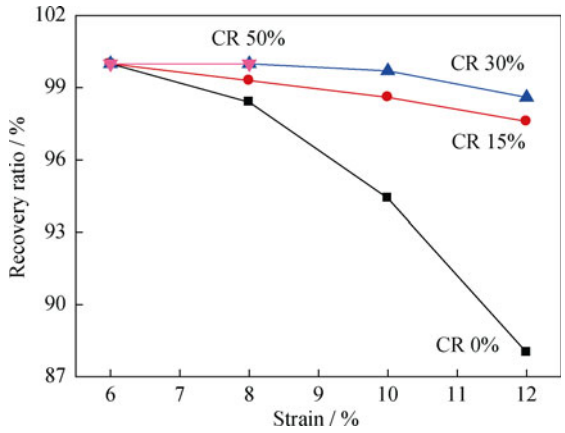

Fig. 5 Strain dependence of shape-recovery ratio of $Ti_{50}Ni_{49}Fe_1$ alloy (curve for alloy with CR 50 % being only from 6 % to 8 % owing to the failure of sample)

to be a measure of the resistance of the grain boundary to slip transfer.

At the same time, although the alloy is suffered certain amount of decrement, the $Ti_{50}Ni_{49}Fe_1$ alloy with cold-rolling still has a relatively high level elongation of 12 %. For shape memory alloys, shape memory effect is another vitally important parameter to evaluate the mechanical properties of these materials. To characterize the influence of cold rolling on the TiNiFe shape memory alloys, the shape memory effect of $Ti_{50}Ni_{49}Fe_1$ alloys with CR0 %, CR15 %, and CR30 % were tested.

As shown in Fig. 5, the recovery strain increases with pre-strain level increasing, and the maximum complete recovery strain value of 8.8 % is obtained in CR30 % alloy. Moreover, the recovery ratio of the hot rolled alloy drastically decreases with pre-strain level increasing. It reduces to ~88 % with pre-strain of 12 %, while that of CR30 % alloy maintains relatively high recovery ratio—above 98 %. As we know, stress over yield stress (σ_S) leads to plastic deformation, which results in irreversible strain of alloys. As seen from Fig. 4, σ_S of the cold-rolled alloys are obviously increased. Therefore, higher stress is required to generate plastic deformation. In such a case, the shape memory effects of cold-rolled alloys get enhanced compared with hot-rolled alloy.

4 Conclusion

In this work, shape memory alloy $Ti_{50}Ni_{49}Fe_1$ cold-rolled by SPD (0 %, 15 %, 30 %, 50 %) was investigated. There are no martensitic phase transformations when the deformation is up to 30 %. And the amount of R phase decreases with the increase of SPD due to the enlargement of temperature interval for R-phase transformation. After cold-rolling, the alloy is mainly composed by B2 parent phases, some stress-induced martensitic B19′ phases occur, and then high density of dislocations are generated, which result in the obvious refinement of grains in the alloys. The yield stress σ_b significantly increases from 618 MPa with CR0 % to 1,338 MPa with CR50 %, respectively. The elongation decreases and remains 12 % for 50 % SPD. Shape memory effect of 30 % SPD increases from 6.5 % of CR0 % to 8.5 % after CR30 %. Therefore, the SPD is beneficial for mechanical properties of shape-memory alloy $Ti_{50}Ni_{49}Fe_1$.

Acknowledgments This study was financially supported by the National Natural Science Foundation of China (No. 50921003) and the Industry, Education and Research Projects of the China Aviation Industrial (No. cxy2012BH04).

References

[1] Otsuka K, Wayman CM. Shape Memory Materials. Cambridge: Cambridge University Press; 1998. 49.
[2] Otsuka K, Ren X. Physical metallurgy of Ti–Ni-based shape memory alloys. Prog Mater Sci. 2005;50(5):511.
[3] Sui JH, Gao ZY, Li YF, Zhang ZG, Cai W. A study on NiTiNbCo shape memory alloy. Mater Sci Eng A. 2009;508(1):33.

[4] Jiang F, Liu Y, Yang H, Li L, Zheng YF. Effect of ageing treatment on the deformation behaviour of Ti–50.9 at% Ni. Acta Mater. 2009;57(16):4773.
[5] Kim JI, Miyazaki S. Effect of nano-scaled precipitates on shape memory behavior of Ti-50.9 at% Ni alloy. Acta Mater. 2005;53(17):4545.
[6] Valiev RZ, Islamgaliev RK, Alexandrov IV. Bulk nanostructured materials from severe plastic deformation. Prog Mater Sci. 2000;V45(2):103.
[7] Urbina C, De la Flor S, Ferrando F. Effect of thermal cycling on the thermomechanical behaviour of NiTi shape memory alloys. Mater Sci Eng A. 2009;501(1):197.
[8] Gall K, Maier HJ. Cyclic deformation mechanisms in precipitated NiTi shape memory alloys. Acta Mater. 2002;50(18):4643.
[9] Valiev R. Nanostructuring of metals by severe plastic deformation for advanced properties. Nat Mater. 2004;3(8):511.
[10] Valiev RZ, Alexandrov IV. Nanostructured materials from severe plastic deformation. Nanostruct Mater. 1999;12(1):35.
[11] Alexandrov IV, Valiev RZ. Nanostructures from severe plastic deformation and mechanisms of large-strain work hardening. Nanostruct Mater. 1999;12(5):709.
[12] Brailovski V, Prokoshkin SD, Khmelevskaya IY, Inaekyan KE, Demers V, Dobatkin SV, Tatyanin EV. Structure and properties of the Ti-50.0 at% Ni alloy after strain hardening and nanocrystallizing thermomechanical processing. Mater Trans. 2006;47(3):795.
[13] Brailovski V, Prokoshkin SD, Khmelevskaya IY, Inaekyan KE, Demers V, Bastarache E, Dobatkin SV, Tatyanin EV. Interrelations between the properties and structure of thermomechanically-treated equiatomic Ti–Ni alloy. Mater Sci Eng A. 2006;438:597.
[14] Prokoshkin SD, Brailovskii V, Khmelevskaya IY, Dobatkin SV, Inaekyan KE, Turilina VY, Demers V, Tat'yanin EV. Creation of substructure and nanostructure in thermomechanical treatment and control of functional properties of Ti–Ni alloys with shape memory effect. Met Sci Heat Treat. 2005;47(5–6):182.
[15] Tsuchiya K, Inuzuka M, Tomus D, Hosokawa A, Nakayama H, Morii K, Todaka Y, Umemoto M. Martensitic transformation in nanostructured TiNi shape memory alloy formed via severe plastic deformation. Mater Sci Eng A. 2006;438:643.
[16] Waitz T, Kazykhanov V, Karnthaler HP. Martensitic phase transformations in nanocrystalline NiTi studied by TEM. Acta Mater. 2004;52(1):137.
[17] Petch NJ. The cleavage strength of polycrystals. J Iron Steel Inst. 1953;174(19):25.